batteries

MDPI

Article

Li-Ion Mobility and Solvation Structures in Concentrated Poly(ethylene carbonate) Electrolytes: A Molecular Dynamics Simulation Study

Wei Tan, Kento Kimura and Yoichi Tominaga *

Graduate School of Bio-Applications and Systems Engineering, Tokyo University of Agriculture and Technology, 2-24-16 Naka-cho, Koganei-shi, Tokyo 184-8588, Japan; tanwei96@st.go.tuat.ac.jp (W.T.); kento-kimura@go.tuat.ac.jp (K.K.)
* Correspondence: ytominag@cc.tuat.ac.jp

Abstract: With the rapid global increase in the use of digital devices and electric vehicles, solid polymer electrolytes (SPEs) have emerged as promising candidates for all-solid-state batteries. They are expected to resolve safety concerns and overcome the limitations of energy density and charging speed associated with traditional Li-ion batteries with liquid electrolytes. However, a limited understanding of ionic conduction mechanisms remains a significant barrier to their further development and practical application. In this study, we employed molecular dynamics simulations using the COMPASS II force field under NPT/NVT ensembles at 298 K to investigate the static and dynamic properties of poly(ethylene carbonate) (PEC) electrolytes at various salt concentrations. Key analyses included the radial distribution function, solvation free energy, and mean-square displacement (MSD) of individual Li cations. Based on their MSD data, Li cations were categorized into "faster" or "slower" groups, corresponding to conductivity levels above or below the average in each model. Our findings reveal that, at higher concentrations, a smaller fraction of faster Li cations contributes disproportionately more than slower Li cations to the overall mobility, highlighting that targeted manipulation of solvation structures could enhance ion transport efficiency in highly concentrated SPEs. Additionally, changes in coordination number and solvation free energy for both faster and slower Li cations suggest the existence of three different solvation patterns as salt concentration increases. These insights provide a deeper understanding of ionic transport and solvation structures in PEC electrolytes, with potential implications for the design of more efficient all-solid-state batteries.

Keywords: solid polymer electrolyte; poly(ethylene carbonate); lithium battery; molecular dynamics; mean-square displacement; solvation free energy

Academic Editor: Claudio Gerbaldi

Received: 26 November 2024
Revised: 22 January 2025
Accepted: 25 January 2025
Published: 28 January 2025

Citation: Tan, W.; Kimura, K.; Tominaga, Y. Li-Ion Mobility and Solvation Structures in Concentrated Poly(ethylene carbonate) Electrolytes: A Molecular Dynamics Simulation Study. *Batteries* **2025**, *11*, 52. https://doi.org/10.3390/batteries11020052

1. Introduction

With the continuous and rapid development of digital technologies, the demand for energy storage devices such as rechargeable Li-ion batteries is increasing. However, commercial liquid electrolytes pose risks to safety due to their relatively low flammability and potential leakage [1]. Solid polymer electrolytes (SPEs) offer an inherently safer alternative and hold promise for addressing these safety concerns in Li-ion batteries [2]. SPEs are able to exist stably with Li anodes and can potentially prevent the formation of Li dendrites. As a result, they allow for a higher energy density and increased safety in all-solid-state Li-ion batteries [3]. Compared to inorganic solid electrolytes, polymer-based electrolytes offer advantages such as simpler production, cost-effectiveness, greater

workability, and enhanced mechanical toughness [4]. Therefore, SPEs are considered strong candidates for use in all-solid-state batteries [5]. Nonetheless, despite significant advances, polymers like poly(ethylene oxide) (PEO) still have comparatively lower ionic conductivity compared to liquid or inorganic solid electrolytes [6].

PEO was the first polymer matrix used for SPE where ionic conductivity was experimentally measured [7], and earlier research on polymer electrolytes demonstrated a close relationship between polymer structure and ionic conductivity, highlighting how polymer-specific properties such as glass transition temperature (T_g) and segmental mobility relate to ion transport. Many experiments and molecular simulation studies have been designed to shed light on the mechanisms behind ionic conduction in polymer electrolytes [8]. For example, Guo et al. used electrochemical methods and molecular simulations based on the Monte Carlo method in the composite polymer electrolytes model to investigate ionic conduction, showing that at the interfaces between different phases, ionic conduction is predominantly influenced by space-charge regions [9]. Some studies focused on the role of temperature in conductivity, from which they developed and applied the dynamic bond percolation (DBP) theory in molecular dynamics (MD) simulations [10,11]. Borodin et al. conducted MD and other Monte Carlo method simulations on PEO-based electrolytes, explaining charge migration within the PEO/Li^+ system through the renewal of hopping probabilities [12]. Ganesan et al. examined the influence of SiO_2 nanoparticles on ion transport within PEO/$LiBF_4$/SiO_2 composite polymer electrolytes using MD simulations, showing that the addition of nanoparticles reduced the overall ionic conductivity as the result of a decrease in segmental motion in polymer chains [13].

Understanding the mechanisms of fast ionic conduction and accurately predicting ionic conductivity are essential for the design and development of SPEs. The related studies can capture some unique features from polymers or SPEs, such as T_g and the mobility of segmental polymer chains, and connect them to ionic conductivity. In our previous studies, we have investigated novel poly(alkylene carbonate) electrolytes, particularly poly(ethylene carbonate) (PEC), which are promising candidates, due to their excellent salt solvation capabilities and unusual T_g behavior, which play a key role in their unique ionic conduction performance [14]. Compared to conventional PEO-based SPEs, PEC exhibits weaker Li^+-polymer coordination due to its carbonate backbone, which prevents the formation of overly stable solvation structures observed in PEO systems [14,15]. Moreover, PEC can offer potential environmental benefits by utilizing carbon dioxide through the polymerization of carbon dioxide and epoxides [16,17].

Achieving high ionic conductivity is critical for solid electrolytes, and ongoing efforts aim to enhance this property while maintaining other important characteristics [18]. A key challenge in studying ion transport in SPEs, especially in concentrated electrolyte systems, is understanding how ion solvation impacts transport properties at higher concentrations. This challenge has become even more critical with recent advances in computational capabilities, which now allow for more accurate analysis of transport properties [19–21]. In our previous simulation studies, we calculated the free volume and Li-ion coordination numbers of PEC and lithium bis(trifluoromethanesulfonyl) imide, the safe and polar Li salt known as LiTFSI, at various concentration ratios using radial distribution functions (RDFs) [22]. With the changes in coordination numbers, we found that the interactions between the Li cations and polymer chains weakened as the Li salt concentration of increased. However, these interactions were still sufficient to promote the dissociation of ion pairs, maintaining a high concentration of free ions in the electrolyte while preventing the formation of overly stable coordination structures similar to those observed in PEO-based electrolytes [23]. Comparing these results with FT-IR data [24], we also observed a consistent increase in free volume, in line with FT-IR findings on aggregated ion groups,

indicating that the formation of aggregated ions ultimately leads to an increase in free volume, improving both Li cation and polymer segment mobility, and thus enhancing ionic conductivity.

In this study, we investigated the distribution of diffusivity for each Li cation in PEC/LiTFSI electrolyte models with different Li salt concentrations and therefore classified the Li cations into "faster" and "slower" groups, enabling a direct link between dynamic behavior and solvation chemistry. The coordination numbers and solvation free energies (SFEs) of these two groups were examined at various electrolyte concentrations to gain a comprehensive understanding of how coordination chemistry and solvation effects influence ion transport properties in the electrolytes.

2. Computational Details

2.1. Modeling and Structure Optimization

The electrolyte models were constructed with Materials Studio (MS) 7.0 program following a stepwise procedure, as established in our previous study [22]. First, an ethylene carbonate (EC) monomer model was created, along with individual models for the Li cation (Li^+) and the bis(trifluoromethanesulfonyl) imide anion ($TFSI^-$). Each of these models was then individually optimized for energy and structure using the B3LYP/6-31++G** method based on Gaussian basis sets. Afterward, an EC unit was generated from the optimized EC monomer, and poly(ethylene carbonate) (PEC) polymer chains, each composed of 20 EC units, were formed. In the next step, 10 chains of PEC were filled with LiTFSI salt ions. All the LiTFSI ions were added as separate Li^+ or $TFSI^-$ ions in quantities corresponding to specific concentrations of x mol% (x = 5, 10, 20, 40, 60, 80, 100, and 120), and were placed into a simulation box using the Amorphous Cell module (600 carbon atoms, 804 hydrogen atoms, and 602 oxygen atoms were contained in each model, and organized into 10 polymer chains). The Amorphous Cell module employs a Monte Carlo method to generate a pseudo amorphous model with periodic boundary conditions, which offers an approach to the multiscale modeling of polymer systems that can both predict the deformation of polymer chains and scale up the size of the model without excessive computational costs [25]. Finally, two successive molecular dynamics (MD) simulations were performed for each amorphous model: the first under NPT (conserved number of atoms, pressure, and temperature) ensemble and the second under NVT (conserved number of atoms, volume, and temperature) ensemble, both at 298 K, to ensure equilibrium within each system. Chemical structures and optimized models of PEC and $TFSI^-$ ion are illustrated in Figure 1, and more details on NPT simulations can be found in Table S1.

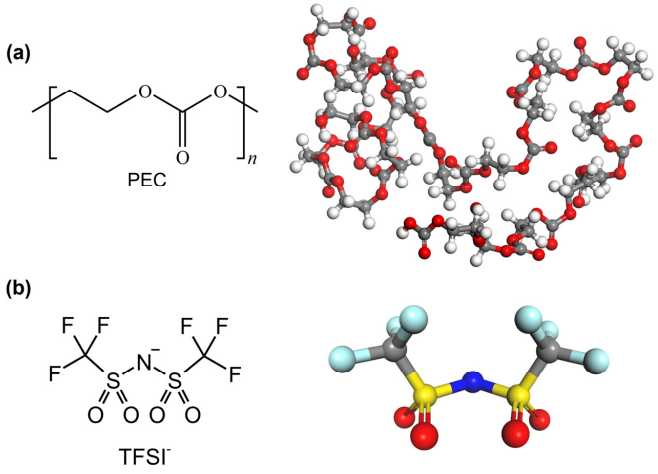

Figure 1. Chemical structures and molecular models of (**a**) PEC chain and (**b**) $TFSI^-$ ion.

2.2. Computational Methods

The simulations in this study, including the modeling and structure optimization steps mentioned earlier, were performed in the Materials Studio 7.0 program package and its built-in modules [26]. Specifically, all MD simulations were carried out using the Forcite module with the 2.8 version of COMPASS molecular force field (COMPASS II). Forcite is an advanced classical molecular mechanics tool used to perform a wide range of fast energy calculations and reliable molecular mechanics calculations, such as geometry optimization, molecular dynamics, and annealing. COMPASS (Condensed-phase Optimized Molecular Potentials for Atomistic Simulation Studies) is a widely used force field that relies on a massive number of empirical parameters and is scaled from ab initio HF/6-31G* simulations [27,28]. COMPASS II is part of the MS 7.0 program package and is particularly effective for atomistic simulations of organic compounds, inorganic molecules, and polymers. With COMPASS, Fried et al. investigated four gas molecules in poly(2,6-dimethyl-1,4-phenylene oxide) and examined their self-diffusion and solubility coefficients [29]. Ernesto et al. constructed an ionic-conducting polymer–electrolyte system with COMPASS and described the ionic conductivity mechanism of H_3O^+ and OH^- along the polymer matrix [30].

Considering the balance between accuracy and computational cost required for different aspects of this study, we carefully selected the appropriate functionals and methods for each technique, as detailed below. The force field was set to COMPASS II, and all of the partial atomic charges were assigned by the COMPASS II force field. The summation method for electrostatic interactions was set to *Ewald* with an accuracy of 0.001 kcal/mol. For the interactions of van der Waals forces, the *Atom-based* method was employed with a cutoff distance of 12.5 Å. The pressure for NPT simulations was maintained at 0.0001 GPa using the *Berendsen* barostat, with a relaxation time constant of 0.1 ps. During the NPT and NVT simulations, the temperature was kept at around 298 K using a *Nosé-Hoover* thermostat, also with a 0.1 ps relaxation time. Each MD process continued from the final structure of the preceding simulation, ensuring a smooth transition between the NPT, NVT, and NVE (conserved number of atoms, volume, and energy) simulations. To guarantee that the models reached equilibrium, a simulation time of 2000 ps was used for each MD process, with an integration time step of 1 fs. To better analyze the mean-square displacement (MSD) of Li cations and distinguish between faster and slower Li cations, a snapshot of the model was saved every 1 ps during the simulations.

2.3. Mean-Square Displacement

Ionic conductivity (σ) is one of the most crucial properties for assessing the conductive performance of polymer electrolytes. When discussing the behavior of Li cations, the conductivity is simply directly proportional to the self-diffusion coefficient (D) of those Li cations, which represents their diffusion capability, as shown in Equation (1). Furthermore, the value of D is related to the mean-square displacement according to Equation (2). Thus, for simplicity, by calculating the ΔMSD of Li cations, we can effectively compare the conductive capacities of individual Li cations within the same model. In line with our recent studies, we directly computed the ΔMSD of Li cations using NVE MD simulations with a simulation time of 1000 ps and a sampling step of 1 ps.

$$\sigma(m) = \frac{q(m)^2 \rho(m) D(m)}{k_B T} \tag{1}$$

$$D = \lim_{t\to\infty} \frac{1}{6Nt} \sum_{m=1}^{N} [r_m(t) - r_m(0)]^2 = \lim_{t\to\infty} \frac{\mathrm{MSD}(t) - \mathrm{MSD}(t_0)}{6(t - t_0)} = \lim_{t\to\infty} \frac{\Delta\mathrm{MSD}}{6\Delta t} \tag{2}$$

where $q(m)$ is the charge of ion m, $\rho(m)$ is the number density of ions m in the system defined as the ratio of N (the total number of ions m) to the box volume in Table S1 for each model, k_B is the Boltzmann constant, T is the absolute temperature, t is the simulation time, $r_m(t)$ is the recent position of ion m at simulation time t, and $r_m(0)$ is the initial position of ion m.

Finally, for each kind of Li cation m, its transport number $t_+(m)$ is calculated from the distribution of Li cations and anions in the total conductivity, as shown below:

$$t_+(m) = \frac{q_+\sigma_+(m)}{q_+\sigma_+ + q_-\sigma_-} \tag{3}$$

where q_+ is the charge of the Li cation, q_- is the charge of the TFSI anion, $\sigma_+(m)$ is the ionic conductivity of the Li cation m, σ_+ is the ionic conductivity of all Li cations, and σ_- is the ionic conductivity of all TFSI anions. This equation describes the fraction of the total conductivity attributed to the Li cation m in the system. We will use it to analyze the differences between the faster and slower Li cations.

2.4. Coordination Number

The radial distribution function (RDF) is the core measure for polymer electrolytes, as it provides insight into the local environment and coordination structure around each atom or ion. In this study, the RDF was utilized to examine the ionic solvation structure in PEC/LiTFSI electrolytes, especially in concentrated models. In MS, the RDF is represented as a function $g(r)$, which was computed using data from the last 100 ps of the NPT simulations described in Section 2.1. The RDF for any given atom can be defined using the following equation:

$$g(r) = \frac{n(r)}{4\pi r^2 \rho dr} \tag{4}$$

where for every Li cation, $n(r)$ is the total number of surrounding atoms within a shell at a distance between r and $r+dr$, $4\pi r^2$ is the solvation area of the shell, and ρ is the number density of Li-ion's surrounding atoms as previously defined in Equation (2).

It is evident that in this study, by specifying a cutoff distance that satisfies the coordination distance, the coordination number (CN) of a Li cation, denoted as $n(r')$, can be defined using the following integral equation:

$$n(r') = 4\pi\rho \int_0^{r'} g(r) r^2 dr \tag{5}$$

where r' is the x-axis value of the trough immediately after the first peak (means the first coordination sphere) in $g(r)$.

2.5. Solvation Free Energy

In the Forcite module, the solvation free energy (SFE) task calculates the reversible work needed to transfer a solute from the gas phase into the solvation system. This solvation process is determined through three distinct steps: first, the solute molecule in the gas phase is discharged, and the associated free energy change is calculated. Next, the neutralized solute molecule is introduced to the fully charged solvent, and the free energy change for this interaction is determined. Finally, the solvated but uncharged solute molecule is recharged in the solvent environment, and the associated free energy is computed. Each of these three steps involves a series of molecular dynamics calculations, with the Helmholtz free energy changes obtained representing the ideal contribution, van der Waals contribution, and electrostatic contribution to the total solvation free energy of the system [26]. The total solvation free energy is the sum of the free energies from these three processes.

In these calculations, the force field is modified using coupling parameters, which are initially set to 0 and gradually increased to 1 by the end, with a total of 10 steps to simulate the complete solvation process. Additionally, there are two algorithms that can be employed to compute free energy: thermodynamic integration and the acceptance ratio method. In the case of thermodynamic integration, the free energy derivative is computed during each MD simulation run and integrated after completing the steps of the coupling parameter [31]. On the other hand, the acceptance ratio method assesses the likelihood of accepting changes to nearby coupling parameter values, from which the free energy is extracted [32]. The thermodynamic integration method was used, and the NVT ensemble for the MD simulation was specified to obtain Helmholtz free energy. The equilibration and production phases were set to 1000 steps and 5000 steps, respectively, to ensure the accurate integration of the derivative. Additionally, to mitigate the impact of scale differences across different models on the SFE, we computed the Helmholtz free energy between solid-state Li cations and gas-phase Li cations for each model as a correction factor, as shown in Figure 2. Therefore, this comprehensive thermodynamic process pertains to the solvation effect of solid-state Li cations rather than their gas-phase counterparts, as given in Equation (6).

$$\Delta A_{SFE} = \Delta A_{sub} + \Delta A_{id} + \Delta A_{vdw} + \Delta A_{elec} \quad (6)$$

where ΔA_{SFE} is the total solvation free energy describing the progression from solid-state Li cation to dissolved Li cation, ΔA_{sub} is the free energy from the transition of solid-state Li cation to gas-phase Li cation, ΔA_{id} is the free energy of the neutralization from gas-phase Li cation to Li atom, ΔA_{vdw} is the free energy determined by the addition of the neutralized Li to a simulation box, and ΔA_{elec} is the free energy caused by the return of the charges removed from the Li cation.

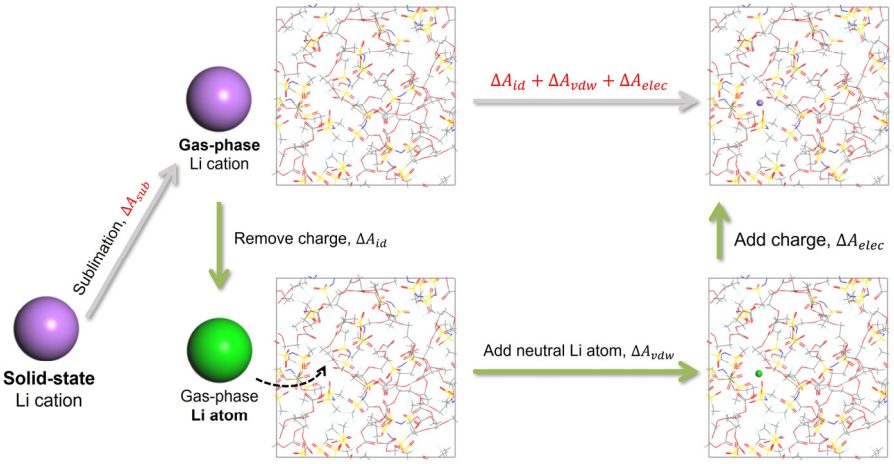

Figure 2. Thermodynamic process for calculating solvation free energy.

3. Results and Discussion

3.1. Mobility of Li Cations

The MSD data for all Li cations, specifically for each Li cation individually, and their averages were obtained from the PEC/LiTFSI electrolyte models, which ranged from 5 mol% to 120 mol% through MD simulations. Figure 3 illustrates the distribution or, in statistics, the probability density of ΔMSD for Li ions in the SPE models at these three concentrations. Meanwhile, for ease of observation, the MSD data are shown for three specific concentrations (20 mol%, 80 mol%, and 120 mol%) in Figure S1. The comparison of ionic conductivities between calculations and experiments was also listed in Table S2 to show the accuracy of simulations. We found that for most Li cations, their ΔMSD values

fall below the overall expected ΔMSD value of all Li cations calculated from the probability densities. With this in mind, we categorized the Li cations in the model into two groups based on whether their ΔMSD values exceed the expected ΔMSD value of all Li cations: those exceeding the expected value were classified as "faster" (or "F" for short), while those below it were classified as "slower" (or "S"). "Overall" (or "O") represents all Li cations collectively. This allowed us to conduct further analysis of the data for each group. For example, the proportion of slower Li cations increases with increasing salt concentration, and the proportion of faster Li cations decreases. This suggests that the mobility differences between faster and slower Li cations within the models also become more pronounced as the salt concentration increases, and it also implies that the variance in the energy levels of the Li cations increases with the concentration. In other words, the solvation environments of the Li cations within the models begin to show greater disparities as the concentration increases.

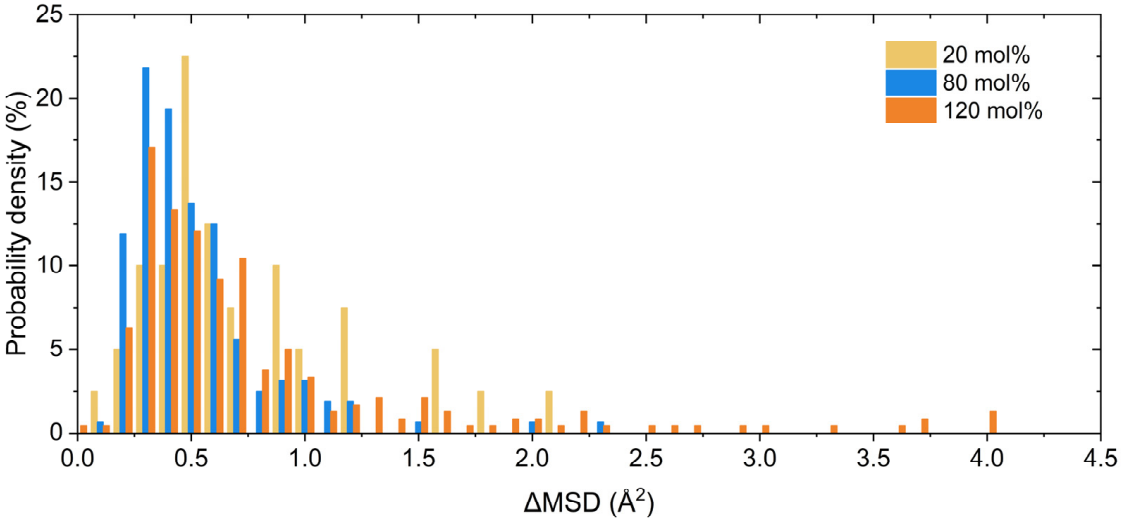

Figure 3. Probability density of ΔMSD for each Li cation calculated in PEC/LiTFSI models, with different salt concentrations of 20 mol%, 80 mol%, and 120 mol%.

3.2. Contribution of Faster Group

After distinguishing between the faster and slower Li cations, we proceeded to calculate the changes in the number proportion of faster Li cations in each group using the previously obtained MSD data. The results are presented in Figure 4 and show that the number proportion of faster Li cations decreases with increasing salt concentrations. Furthermore, as mentioned earlier, the transport numbers of each kind of Li cation, with faster ions denoted as t_+(F) and slower ions denoted as t_+(S), were calculated, and the results are shown in Figure 5. As a comparison to the decreasing number proportion of the faster group, the contribution ratio of t_+(F) to the total transport number of overall Li cations is also shown in Figure 4. It is evident that despite the decrease in the relative number of faster Li cations, their contribution to the transport number consistently remains around 70%. This demonstrates that, at high concentrations, the ion transport efficiency of faster Li cations is significantly higher than that of slower Li cations. This result aligns with the ratio of the conductivities between faster and slower Li cations, which were denoted as D(F) and D(S), respectively. This ratio is shown as relative conductivity in Figure 5, which is approximately 10:1 at high salt concentrations.

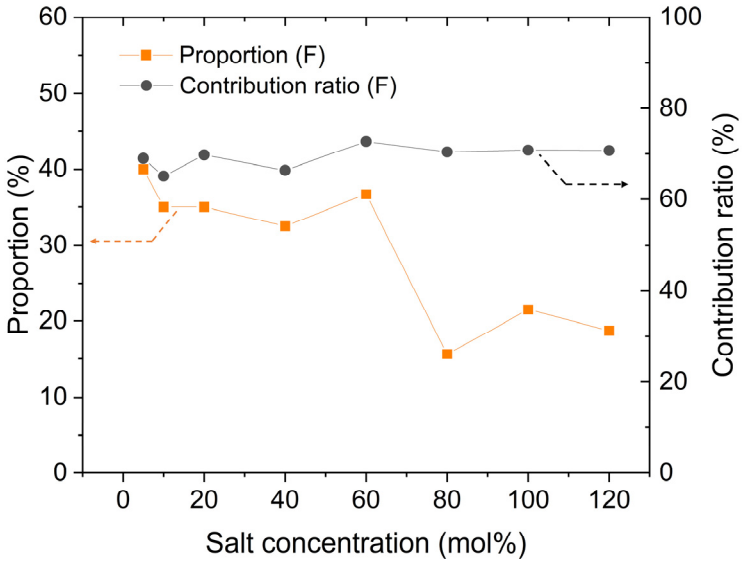

Figure 4. Changes in number proportion and contribution ratio of t_+(F) with different salt concentrations.

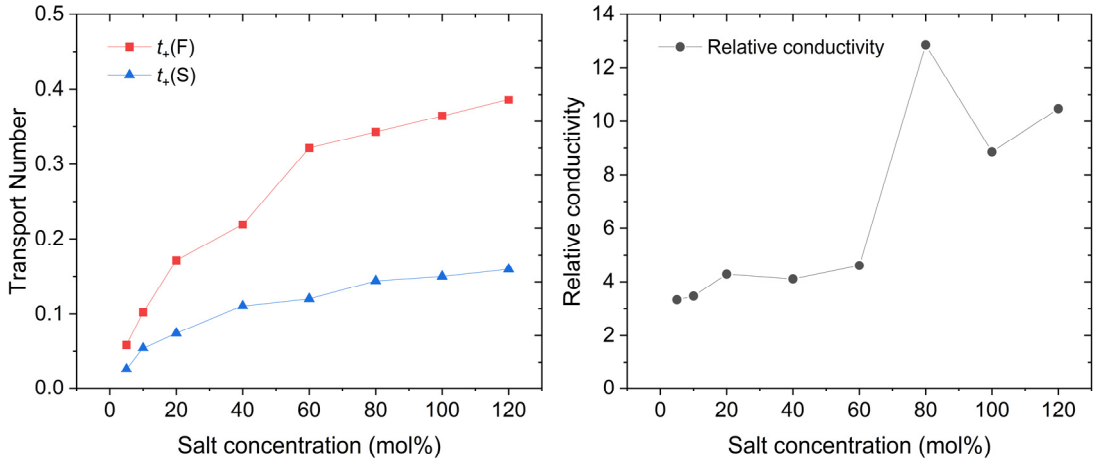

(**a**) (**b**)

Figure 5. Changes in (**a**) the transport number of faster and slower Li cations with different salt concentrations, with t_+(F) in red and t_+(S) in blue, and (**b**) the ratio of D(F) to D(S).

Similar to highly concentrated ionic liquids, highly concentrated SPEs contain a certain number of tight ion pairs and aggregated ions [33,34], which do not directly contribute to conductivity. Therefore, the actual conductivity is primarily provided by free ions [35]. This suggests that the proportion of free Li ions (Li cations that are not limited by coordination effects) among the faster Li cations (free Li ions and Li cations limited by fewer coordination effects) is significantly higher in high-concentration SPEs. Consequently, by studying the faster group of Li cations, we can further investigate the solvation structure of both free and non-free Li ions within the PEC/LiTFSI electrolyte. For example, we can calculate the coordination number (CN) between various Li cations and the carbonyl oxygen atoms on the PEC polymer backbone, as well as with the oxygen atoms in the TFSI anion (denoted as O(PEC) and O(TFSI), respectively), using the radial distribution function (RDF) method. This allows us to further investigate their coordination environments in the solvation state. The results of the coordination number calculations of each kind of Li cation, with faster Li cations denoted as CN(F), slower Li cations denoted as CN(S), and overall Li cations denoted as CN(O), are presented in Figures 6 and 7. For reference, the specific data for these figures are listed in Tables S3–S5. For the faster group, the CN with O(PEC) are lower than

those of the slower group at nearly all concentrations, except for 40 mol%. In our previous study, we mentioned that the presence of O(TFSI) creates a competitive relationship for coordination with O(PEC) [22]. This factor results in the coordination effects of Li cations being less pronounced, regardless of whether they coordinate with O(PEC) or O(TFSI), thus preventing the formation of stable solvation structures similar to those in PEO. The data in Figure 7 indicate that this factor is more pronounced for faster Li cations, as they exhibit lower CNs for O(TFSI), with this trend becoming more significant at higher concentrations. We think that this competitive effect contributes to the noticeable increase in the proportion of freer ions among faster Li cations in high salt concentration electrolytes.

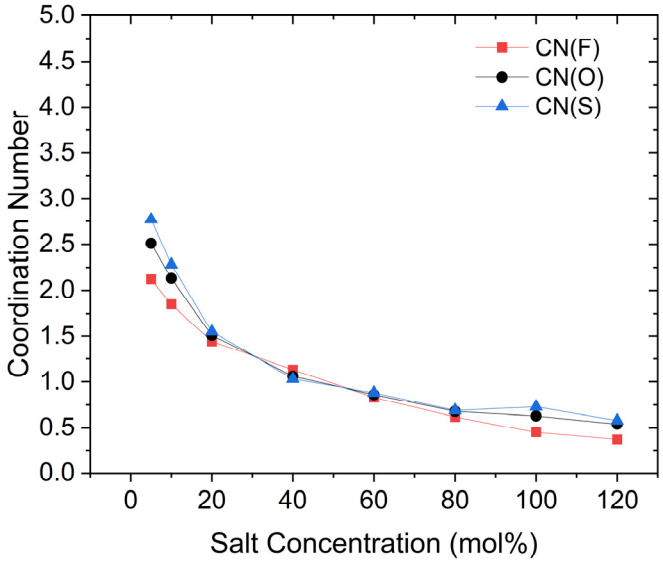

Figure 6. Changes in coordination number between O(PEC) and Li cations with different salt concentrations, with the faster group in red, the slower group in blue, and the overall Li cations in black.

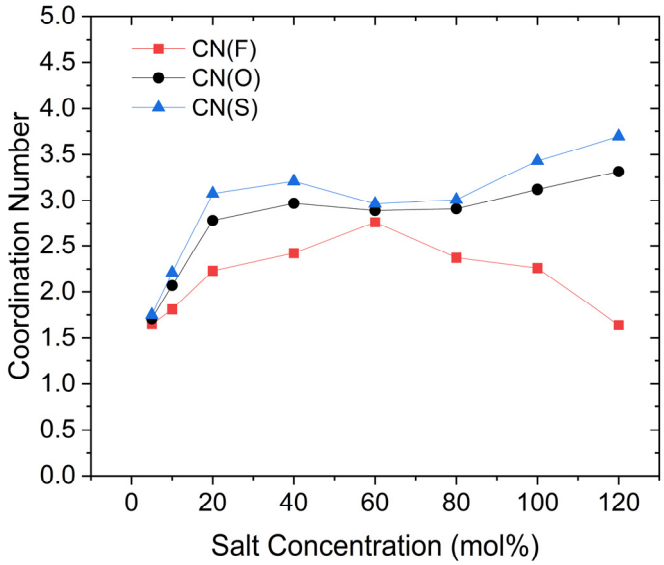

Figure 7. Changes in coordination number between O(TFSI) and Li cations with different salt concentrations, with the faster group in red, the slower group in blue, and the overall Li cations in black.

3.3. Solvation Structures

The solvation free energy (SFE) of Li cations in the PEC/LiTFSI electrolyte system was calculated using the Forcite module, and the results are presented in Figure 8. In total, the value of SFE of Li cations increases with rising salt concentration, indicating that the solvation effect is gradually weakening. Notably, the SFE of faster Li cations is significantly higher than that of slower Li cations, suggesting that slower cations are more likely to form solvation structures, which aligns with the earlier observations of changes in coordination numbers. Additionally, we observed a decline in changes in SFE between 40 mol% and 60 mol%, which may be related to the enhanced coordination effect of O(TFSI) as aggregated ions form. According to our previous study, the aggregation of ions begins to saturate around 80 mol% (indicating that, at this concentration, the vast majority of TFSI anions exist in the form of aggregated ions) [22,33]. The bond rotation of TFSI anions within aggregated ions is somewhat restricted, limiting their ability to freely change conformation. Consequently, some TFSI anions may adopt conformations that are almost incapable of coordinating with Li cations [36]. Therefore, TFSI anions added beyond this concentration are less likely to coordinate with Li cations, further diminishing the coordination effect [37].

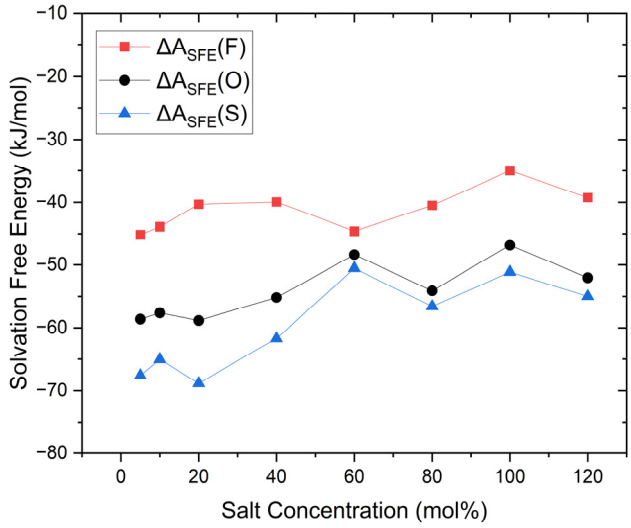

Figure 8. Changes in solvation free energy of Li cations with different salt concentrations, with the faster group in red, the slower group in blue, and the overall Li cations in black.

Upon understanding the changes in the coordination effect of TFSI as the salt concentration increases, we revisit Figure 7 and observe that the coordination number changes of Li-O(TFSI) exhibit a trend nearly opposite to that of SFE. In contrast, the coordination number changes of Li-O(PEC) in Figure 6 display a monotonic and smooth decrease, that is almost independent of SFE variations. Given that SFE changes are closely related to the solvation effect of Li cations, a clear conclusion can be drawn: as salt concentration changes, the SFE of Li cations is primarily influenced by the coordination environment of the Li cations with TFSI anions. At high salt concentrations, in particular, the coordination number between faster Li cations and O(TFSI) decreases significantly, while slower Li cations become more inclined to coordinate with aggregated TFSI anions, occupying the limited coordination sites that remain due to the aggregation effect. Faster Li cations are indeed the primary contributors to ionic conduction in high salt concentration PEC/LiTFSI electrolytes. Considering all the data and observations mentioned above, we can make certain inferences about the solvation environment of faster Li cations in this system: at lower salt concentrations (until 40 mol%), the system predominantly features four-coordination structures with O(PEC) as the main coordinating species. As the salt concentration rises to

40 or 60 mol%, the introduction of TFSI anions and the formation of aggregated ions limit the coordination capacity of O(PEC). Consequently, faster Li cations predominantly adopt three-coordination structures, with O(TFSI) gradually becoming the dominant coordinating species. When the salt concentration exceeds 80 mol%, the absence of isolated TFSI anions leads to a general decline in the coordination abilities of both O(PEC) and O(TFSI) towards Li cations, resulting in a significant presence of two-coordination structures or even simpler structures, i.e., free ions. Based on the three-step changes in the solvation environment, we propose that the faster group of Li ions in the PEC/LiTFSI electrolyte system exhibits three relatively typical solvation structures, as illustrated in Figure 9. These structures undergo mutual transformations as the salt concentration changes.

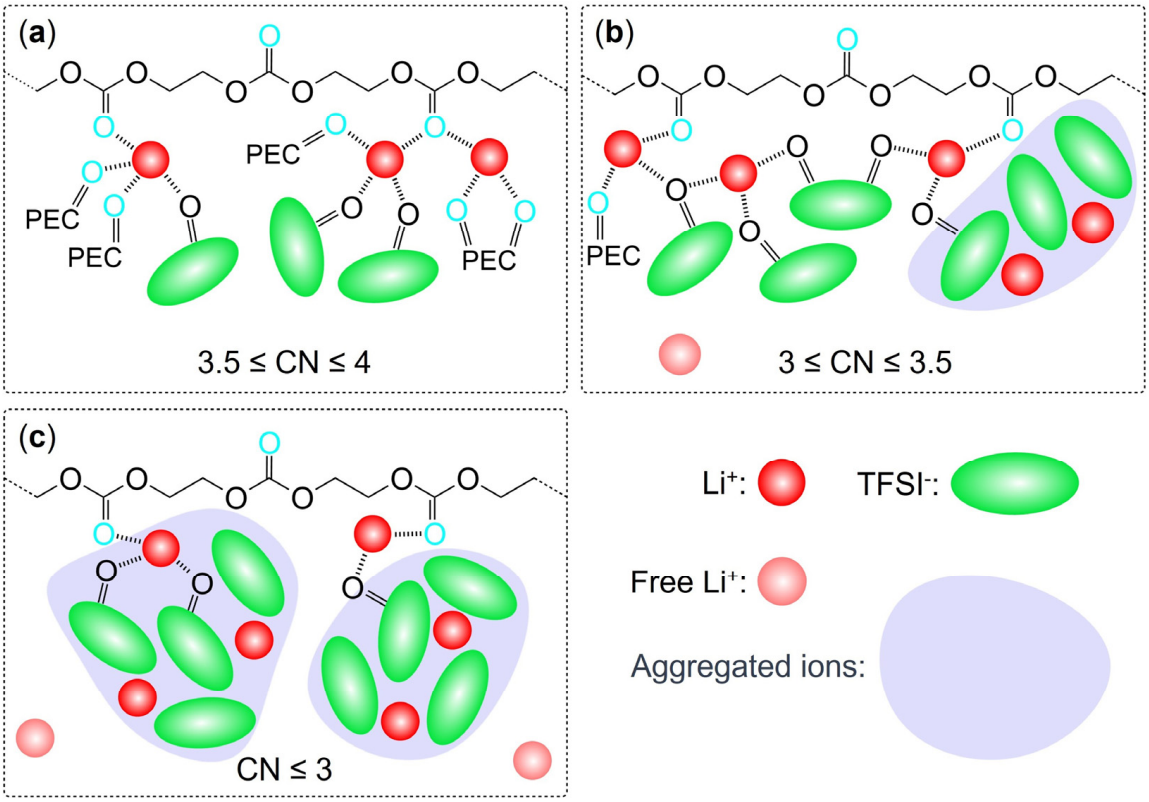

Figure 9. Three typical solvation structures of faster Li cations with different salt concentrations of (**a**) below 60 mol%, (**b**) from 60 mol% to 100 mol%, and (**c**) over 100 mol%. O(PEC) atoms are indicated by light blue.

4. Conclusions

In this study, we employed molecular dynamics-based simulations to obtain intricate experimental data, such as radial distribution functions and solvation free energy, in the PEC/LiTFSI electrolyte system. Our main findings can be summarized as follows:

1. After categorizing Li cations into faster and slower groups based on the mean-square displacement data, their ionic mobility and related characteristics were further analyzed. The results indicated that the faster group has approximately 10 times higher conductivity than the slower group. Consequently, even though the relative quantity of faster Li cations decreases with increasing salt concentration, these ions still contribute around 70% of the cation transport. This suggests that free ions are prevalent among the faster Li cations.
2. By studying the coordination numbers and solvation free energy of the two groups of Li cations, we found that slower Li cations tend to form more coordination structures with oxygen atoms in their environment, while faster Li cations experience less coor-

dination influence. This effect is particularly pronounced at high salt concentrations, at which the coordinating effects from both PEC and TFSI anions weaken due to the formation of aggregated ions, ultimately leading to the emergence of more free ions.

3. Although we are not yet able to establish an exact standard for determining whether a specific Li cation is acting as a free ion during ion transport, the findings of this study have successfully narrowed the range in which Li cations are likely to be free ions. Furthermore, three possible solvation structures for faster Li cations across different salt concentration ranges are proposed, all of which align with the behaviors observed in this study.

These insights will facilitate further research into the mechanism of Li-ion conduction and provide valuable guidance for future development and improvement of electrolyte systems. While the current models have successfully produced conductivity data that align with experimental results, its performance remains constrained by the limitations of available computing resources. These constraints hinder the acquisition of more comprehensive datasets and restrict the ability to replicate the behavior of actual SPEs. Factors such as temperature gradients across the battery and long-range interactions, which could also influence the properties of SPEs, are not yet fully accounted for. Future work will focus on addressing these limitations and enhancing the models to achieve a more accurate representation of SPE materials.

Supplementary Materials: The following supporting information can be downloaded at: https://www.mdpi.com/article/10.3390/batteries11020052/s1, Figure S1. MSDs of each Li cation and average (marked as dashed lines) calculated in PEC/LiTFSI models, with different salt concentrations of (a) 20 mol%, (b) 80 mol%, and (c) 120 mol%; Table S1. Extra parameter details on simulation cubic boxes in NPT simulations; Table S2. Simulated and measured values of ionic conductivities and the expected values of ΔMSD; Table S3. Coordination number of Li-O(PEC); Table S4. Coordination number of Li-O(TFSI); Table S5. Coordination number of Li-O(All). References [38,39] are cited in the Supplementary Materials.

Author Contributions: Methodology, W.T.; Software, W.T.; Formal analysis, W.T.; Writing—original draft, W.T.; Writing—review and editing, K.K. and Y.T.; Funding acquisition, Y.T. All authors have read and agreed to the published version of the manuscript.

Funding: This research was supported financially by a Grant-in-Aid for Scientific Research (B) (23K23057) of JSPS KAKENHI and Data Creation and Utilization-Type Material Research and Development Project (JPMXP1122712807) of MEXT, Japan.

Data Availability Statement: The raw data supporting the conclusions of this article will be made available by the authors upon request.

Conflicts of Interest: The authors declare no conflicts of interest.

References

1. Tarascon, J.M.; Armand, M. Issues and challenges facing rechargeable lithium batteries. *Mater. Sustain. Energy* **2011**, *414*, 171–179.
2. Jim, M. Technology: A solid future. *Nature* **2015**, *526*, S96–S97.
3. Xia, S.; Wu, X.; Zhang, Z.; Cui, Y.; Liu, W. Practical challenges and future perspectives of all-solid-state lithium-metal batteries. *Chem* **2019**, *5*, 753–785. [CrossRef]
4. Zhao, Q.; Stalin, S.; Zhao, C.Z.; Archer, L.A. Designing solid-state electrolytes for safe, energy-dense batteries. *Nat. Rev. Mater.* **2020**, *5*, 229–252. [CrossRef]
5. Fergus, J.W. Ceramic and polymeric solid electrolytes for lithium-ion batteries. *J. Power Sources* **2010**, *195*, 4554–4569. [CrossRef]
6. Zhou, D.; Shanmukaraj, D.; Tkacheva, A.; Armand, M.; Wang, G.X. Polymer electrolytes for lithium-based batteries: Advances and prospects. *Chem* **2019**, *5*, 2326–2352. [CrossRef]
7. Wright, P.V. Electrical conductivity in ionic complexes of poly (ethylene oxide). *Br. Polym. J.* **1975**, *7*, 319. [CrossRef]

8. Shao, Y.Q.; Gudla, H.; Mindemark, J.; Brandell, D.; Zhang, C. Ion transport in polymer electrolytes: Building new bridges between experiment and molecular simulation. *Acc. Chem. Res.* **2024**, *57*, 1123–1134. [CrossRef] [PubMed]
9. Li, Z.; Huang, H.M.; Zhu, J.K.; Wu, J.F.; Yang, H.; Wei, L.; Guo, X. Ionic conduction in composite polymer electrolytes: Case of PEO: Ga-LLZO composites. *ACS Appl. Mater. Interfaces* **2018**, *11*, 784–791. [CrossRef] [PubMed]
10. Nitzan, A.; Ratner, M.A. Conduction in polymers: Dynamic disorder transport. *J. Phys. Chem.* **1994**, *98*, 1765–1775. [CrossRef]
11. Maitra, A.; Heuer, A. Cation transport in polymer electrolytes: A microscopic approach. *Phys. Rev. Lett.* **2007**, *98*, 227802. [CrossRef]
12. Chen, J.; Wu, J.W.; Wang, X.D.; Zhou, A.A.; Yang, Z.L. Research progress and application prospect of solid-state electrolytes in commercial lithium-ion power batteries. *Energy Storage Mater.* **2021**, *35*, 70–87. [CrossRef]
13. Li, Z.; Fu, J.L.; Zhou, X.Y.; Gui, S.W.; Wei, L.; Yang, H.; Li, H.; Guo, X. Ionic conduction in polymer-based solid electrolytes. *Macromolecules* **2015**, *48*, 2773–2786. [CrossRef] [PubMed]
14. Kimura, K.; Tominaga, Y. Understanding electrochemical stability and lithium ion-dominant transport in concentrated poly (ethylene carbonate) electrolyte. *ChemElectroChem* **2018**, *5*, 4008. [CrossRef]
15. Yue, L.; Ma, J.; Zhang, J.; Zhao, J.; Dong, S.; Liu, Z.; Cui, G.; Chen, L. All Solid-State Polymer Electrolytes for High-Performance Lithium Ion Batteries. *Energy Storage Mater.* **2016**, *5*, 139. [CrossRef]
16. Sugimoto, H.; Inoue, S. Recent Progress in the Synthesis of Polymers Based on Carbon Dioxide. *Pure Appl. Chem.* **2006**, *78*, 1823. [CrossRef]
17. Klaus, S.; Lehenmeier, M.W.; Anderson, C.E.; Rieger, B. Recent advances in CO_2/epoxide copolymerization—New strategies and cooperative mechanisms. *Coord. Chem. Rev.* **2011**, *255*, 1460. [CrossRef]
18. Duan, H.; Yin, Y.X.; Zeng, X.X.; Li, J.Y.; Shi, J.L.; Shi, Y.; Wen, R.; Guo, Y.G.; Wan, L.J. In-situ plasticized polymer electrolyte with double-network for flexible solid-state lithium-metal batteries. *Energy Storage Mater.* **2018**, *10*, 85–91. [CrossRef]
19. Fong, K.D.; Self, J.; McCloskey, B.D.; Persson, K.A. Ion correlations and their impact on transport in polymer-based electrolytes. *Macromolecules* **2021**, *54*, 2575–2591. [CrossRef]
20. Vargas-Barbosa, N.M.; Roling, B. Dynamic ion correlations in solid and liquid electrolytes: How do they affect charge and mass transport? *ChemElectroChem* **2020**, *7*, 367–385. [CrossRef]
21. Zhang, Z.D.; Wheatle, B.K.; Krajniak, J.; Keith, J.R.; Ganesan, V. Ion mobilities, transference numbers, and inverse Haven ratios of polymeric ionic liquids. *ACS Macro Lett.* **2020**, *9*, 84–89. [CrossRef] [PubMed]
22. Tan, W.; Tominaga, Y. Modeling analysis of ionic solvation structure in concentrated poly (ethylene carbonate) electrolytes. *Electrochim. Acta* **2023**, *464*, 142875. [CrossRef]
23. Andersson, R.; Hernández, G.; Mindemark, J. Quantifying the ion coordination strength in polymer electrolytes. *Phys. Chem. Chem. Phys.* **2022**, *24*, 16343. [CrossRef] [PubMed]
24. Motomatsu, J.; Kodama, H.; Furukawa, T.; Tominaga, Y. Dielectric Relaxation Behavior of a Poly (ethylene carbonate)-Lithium Bis-(trifluoromethanesulfonyl) Imide Electrolyte. *Macromol. Chem. Phys.* **2015**, *216*, 1660. [CrossRef]
25. Tan, V.B.C.; Zeng, X.S.; Deng, M.; Lim, K.M.; Tay, T.E. Multiscale modeling of polymers–The Pseudo Amorphous Cell. *Comput. Methods Appl. Mech. Eng.* **2008**, *197–198*, 536–554. [CrossRef]
26. *BIOVIA Materials Studio*, 7.0; Dassault Systèmes: San Diego, CA, USA, 2014. Available online: https://www.3ds.com/products/biovia/materials-studio (accessed on 19 November 2024).
27. Sun, H. COMPASS: An ab Initio Force-Field Optimized for Condensed-Phase Applications–Overview with Details on Alkane and Benzene Compounds. *J. Phys. Chem. B* **1998**, *102*, 7338–7364. [CrossRef]
28. Sun, H.; Jin, Z.; Yang, C.W.; Akkermans, R.L.C.; Robertson, S.H.; Spenley, N.A.; Miller, S.; Todd, S.M. COMPASS II: Extended coverage for polymer and drug-like molecule databases. *J. Mol. Model.* **2016**, *22*, 47. [CrossRef]
29. Fried, J.R.; Sadat-Akhavi, M.; Mark, J.E. Molecular simulation of gas permeability: Poly(2,6-dimethyl-1,4-phenylene oxide). *J. Membrane Sci.* **1998**, *149*, 115–126. [CrossRef]
30. López-Chávez, E.; Martínez-Magadán, J.M.; Oviedo-Roa, R.; Guzmán, J.; Ramírez-Salgado, J.; Marín-Cruz, J. Molecular modeling and simulation of ion-conductivity in chitosan membranes. *Polymer* **2005**, *46*, 7519–7527. [CrossRef]
31. Darve, E. Thermodynamic integration using constrained and unconstrained dynamics. In *Free Energy Calculations: Theory and Applications in Chemistry and Biology*; Springer: Berlin/Heidelberg, Germany, 2007; pp. 119–170.
32. Bennett, C.H. Efficient estimation of free energy differences from Monte Carlo data. *J. Comput. Phys.* **1976**, *22*, 245–268. [CrossRef]
33. Kimura, K.; Motomatsu, J.; Tominaga, Y. Correlation between solvation structure and ion-conductive behavior of concentrated poly (ethylene carbonate)-based electrolytes. *J. Phys. Chem. C* **2016**, *120*, 12385. [CrossRef]
34. Li, T.; Zhang, X.Q.; Yao, N.; Yao, Y.X.; Hou, L.P.; Chen, X.; Zhou, M.Y.; Huang, J.Q.; Zhang, Q. Stable anion-derived solid electrolyte interphase in lithium metal batteries. *Angew. Chem. Int. Ed.* **2021**, *60*, 22683–22687. [CrossRef]
35. Feng, G.; Chen, M.; Bi, S.; Goodwin, Z.A.H.; Postnikov, E.B.; Brilliantov, N.; Urbakh, M.; Kornyshev, A.A. Free and bound states of ions in ionic liquids, conductivity, and underscreening paradox. *Phys. Rev. X* **2019**, *9*, 021024. [CrossRef]

36. Li, S.; Cao, Z.; Peng, Y.X.; Liu, L.; Wang, Y.L.; Wang, S.; Wang, J.Q.; Yan, T.Y.; Gao, X.P.; Song, D.Y.; et al. Molecular dynamics simulation of LiTFSI-acetamide electrolytes: Structural properties. *J. Phys. Chem. B* **2008**, *112*, 6398–6410. [CrossRef] [PubMed]
37. Lassègues, J.C.; Grondin, J.; Aupetit, C.; Johansson, P. Spectroscopic identification of the lithium ion transporting species in LiTFSI-doped ionic liquids. *J. Phys. Chem. A* **2009**, *113*, 305–314. [CrossRef] [PubMed]
38. He, Z.J.; Fan, L.Z. Poly(ethylene carbonate)-based electrolytes with high concentration Li salt for all-solid-state lithium batteries. *Rare Met.* **2018**, *37*, 488–496. [CrossRef]
39. Tominaga, Y. Ion-conductive polymer electrolytes based on poly (ethylene carbonate) and its derivatives. *Polym. J.* **2017**, *49*, 291. [CrossRef]